

High-responsivity solar-blind photodetector based on MOCVD-grown Si-doped β -Ga_2O_3 thin film

Yu-Song Zhi(支钰崧), Wei-Yu Jiang(江为宇), Zeng Liu(刘增), Yuan-Yuan Liu(刘媛媛), Xu-Long Chu(褚旭龙), Jia-Hang Liu(刘佳航), Shan Li(李山), Zu-Yong Yan(晏祖勇), Yue-Hui Wang(王月晖), Pei-Gang Li(李培刚), Zhen-Ping Wu(吴真平), Wei-Hua Tang(唐为华)

Citation: Chin. Phys. B, 2021, 30 (**5**): 057301. DOI: 10.1088/1674-1056/abe37a
Journal homepage: http://cpb.iphy.ac.cn; http://iopscience.iop.org/cpb

What follows is a list of articles you may be interested in

Self-powered solar-blind photodiodes based on EFG-grown (100)-dominant β-Ga_2O_3 substrate

Xu-Long Chu(褚旭龙), Zeng Liu(刘增), Yu-Song Zhi(支钰崧), Yuan-Yuan Liu(刘媛媛), Shao-Hui Zhang(张少辉), Chao Wu(吴超), Ang Gao(高昂), Pei-Gang Li(李培刚), Dao-You Guo(郭道友), Zhen-Ping Wu(吴真平), and Wei-Hua Tang(唐为华)

Chin. Phys. B, 2021, 30 (**1**): 017302. DOI: 10.1088/1674-1056/abc546

Synthesis of free-standing Ga_2O_3 films for flexible devices by water etching of $Sr_3Al_2O_6$ sacrificial layers

Xia Wang(王霞), Zhen-Ping Wu(吴真平), Wei Cui(崔尉), Yu-Song Zhi(支钰崧), Zhi-Peng Li(李志鹏), Pei-Gang Li(李培刚), Dao-You Guo(郭道友), Wei-Hua Tang(唐为华)

Chin. Phys. B, 2019, 28 (**1**): 017305. DOI: 10.1088/1674-1056/28/1/017305

Enhanced photoresponse performance in Ga/Ga_2O_3 nanocomposite solar-blind ultraviolet photodetectors

Shu-Juan Cui(崔书娟), Zeng-Xia Mei(梅增霞), Yao-Nan Hou(侯尧楠), Quan-Sheng Chen(陈全胜), Hui-Li Liang(梁会力), Yong-Hui Zhang(张永晖), Wen-Xing Huo(霍文星), Xiao-Long Du(杜小龙)

Chin. Phys. B, 2018, 27 (**6**): 067301. DOI: 10.1088/1674-1056/27/6/067301

Effects of fluorine-based plasma treatment and thermal annealing on high-Al content AlGaN Schottky contact

Fang Liu(刘芳), Zhixin Qin(秦志新)

Chin. Phys. B, 2016, 25 (**11**): 117304. DOI: 10.1088/1674-1056/25/11/117304

Hetero-epitaxy of L_g=0.13-μm metamorphic AlInAs/GaInAs HEMT on Si substrates by MOCVD for logic applications

Huang Jie, Li Ming, Zhao Qian, Gu Wen-Wen, Lau Kei-May

Chin. Phys. B, 2015, 24 (**8**): 087305. DOI: 10.1088/1674-1056/24/8/087305

High-responsivity solar-blind photodetector based on MOCVD-grown Si-doped β-Ga_2O_3 thin film*

Yu-Song Zhi(支钰崧)[1], Wei-Yu Jiang(江为宇)[1], Zeng Liu(刘增)[1,5], Yuan-Yuan Liu(刘媛媛)[2,3], Xu-Long Chu(褚旭龙)[1,4], Jia-Hang Liu(刘佳航)[1], Shan Li(李山)[1], Zu-Yong Yan(晏祖勇)[1], Yue-Hui Wang(王月晖)[1], Pei-Gang Li(李培刚)[1,†], Zhen-Ping Wu(吴真平)[1], and Wei-Hua Tang(唐为华)[1,5,‡]

[1] *Laboratory of Information Functional Materials and Devices, School of Science & State Key Laboratory of Information Photonics and Optical Communications, Beijing University of Posts and Telecommunications, Beijing* 100876, *China*

[2] *Center of Materials Science and Optoelectronics Engineering, University of Chinese Academy of Sciences, Beijing* 100049, *China*

[3] *The Engineering Research Center for Semiconductor Integrated Technology, Institute of Semiconductors, Chinese Academy of Sciences, Beijing* 100083, *China*

[4] *China Aerospace System Simulation Technology Co., Ltd. (Beijing), Beijing* 100195, *China*

[5] *College of Electronic and Optical Engineering & College of Microelectronics, Nanjing University of Posts and Telecommunications, Nanjing* 210023, *China*

(Received 9 December 2020; revised manuscript received 22 January 2021; accepted manuscript online 5 February 2021)

Si-doped β-Ga_2O_3 films are fabricated through metal-organic chemical vapor deposition (MOCVD). Solar-blind ultraviolet (UV) photodetector (PD) based on the films is fabricated by standard photolithography, and the photodetection properties are investigated. The results show that the photocurrent increases to 11.2 mA under 200 $\mu W \cdot cm^{-2}$ 254 nm illumination and $\pm$20 V bias, leading to photo-responsivity as high as 788 $A \cdot W^{-1}$. The Si-doped β-Ga_2O_3-based PD is promised to perform solar-blind photodetection with high performance.

Keywords: Si-doped β-Ga_2O_3, metal-organic chemical vapor deposition (MOCVD), solar-blind, high responsivity

PACS: 73.30.+y, 85.25.Oj, 85.60.Dw **DOI:** 10.1088/1674-1056/abe37a

1. Introduction

Since ultraviolet (UV) radiation was discovered by Johann Ritter in 1801, it has received extensive research for its influence on the survival and development of humankind.[1,2] According to the International Commission on Illumination, the ultraviolet spectrum could be divided into three bands: UVA, UVB, and UVC.[3] Due to the strong absorption of the protective ozone layer, the UVC region is also called as the solar-blind region, which means the noise signal of the UVC radiation in natural background is very weak and the radiation signal could be very accurately detected.[4] Thus, solar-blind photodetectors (PDs) have plenty of applications in flame sensing, information communication, chemical/biological analysis, etc.[5,6] Among various solar-blind photodetectors, Ga_2O_3 is deemed as a promising candidate for UVC detection because of its proper bandgap ($\sim$ 4.9 eV), good reliability, and availability.[7,8] Up to now, various kinds of Ga_2O_3 based PDs are extensively investigated.[9] Metal–semiconductor–metal (MSM) structured devices are fabricated on β, α, and ε phase Ga_2O_3 films to study their photodetective abilities.[10–14] Schottky junction, heterojunction, and van der walls junction between various materials and Ga_2O_3 films are also exploited to explore the relevant photoconductive and photovoltaic properties.[15–21] Metal–oxide–semiconductor field effect transistor structured Ga_2O_3 PDs are also fabricated to investigate their behaviors as solar-blind phototransistors.[22,23] In addition, as the defects and doped elements affect the carrier transport properties significantly, doping could also be an effective way to enhance the performance of PDs.[24–26] For instance, Zhao *et al.* investigated the photoelectric characteristics of Sn-doped Ga_2O_3.[27] Kokubun *et al.*[28] and Tian *et al.*[29] studied the behaviors of In-doped Ga_2O_3 based photodetector. Grundmann *et al.* demonstrated UV PDs based on a Si-doped $(In_xGa_{1-x})_2O_3$ thin film by PLD methods.[30] Cui *et al.*[31] and Wuu *et al.*[32] investigated the photodetector characteristics of Al-doped Ga_2O_3. Zhao *et al.*[33] and Alema *et al.*[34] observed the improved photoelectric performance in Zn-doped β-Ga_2O_3 films. Guo *et al.* investigated the Mg-doped p-type β-Ga_2O_3 thin film for solar-blind ultraviolet photodetector.[35] Moreover, Fang *et al.* fabricated high quality p-type β-Ga_2O_3 films by doping N elements and paved a novel way to fabricate super sensitive oxide semiconductor photodetectors.[36] However, although doping Si elements is as an effective way to enhance the conductivity of Ga_2O_3, reports about Si-doped Ga_2O_3 PDs are limited. Currently, Kim *et al.*[37] and Pearton *et al.*[38] have studied

*Project supported by the National Natural Science Foundation of China (Grant Nos. 61774019 and 51572033), the Fund of State Key Laboratory of Information Photonics and Optical Communications (BUPT), and the Fundamental Research Funds for the Central Universities, China.

†Corresponding author. E-mail: pgli@bupt.edu.cn

‡Corresponding author. E-mail: whtang@bupt.edu.cn

© 2021 Chinese Physical Society and IOP Publishing Ltd

the photoresponse properties of the Si-implanted Ga_2O_3. The metalorganic chemical vapor deposition (MOCVD) is an effective way to deposit Si-doped Ga_2O_3 films.[39] More investigation about the Si-doped Ga_2O_3 PDs is still required.

Thus, in this paper, Si-doped Ga_2O_3 films were deposited on sapphire substrate by MOCVD methods. An MSM structured PDs device was fabricated and the electric behaviors of the device were measured under dark and 254 nm illumination. With *I–V* and *I–t* measurements, the results indicate that Si-doped Ga_2O_3 films have great potential in solar-blind photodetector fields.

2. Experimental details

Si-doped Ga_2O_3 films were deposited on (0 0 0 1) sapphire substrate by MOCVD methods and obtained from Beijing Gallium Family Technology Co., Ltd. Triethylgallium (TEGa), tetraethyl orthosilicate (TEOS), and high purity O_2 were used as metalorganic precursors for Ga elements, Si elements, and oxidation, respectively, while high purity Ar was used as the carrier gas. During the deposition, the flow rates of the TEGa and TEOS were fixed at 490 sccm and 15 sccm, respectively. The pressure of the chamber was kept at 25 Torr and the deposition temperature was set at 590 °C.

To characterize the crystal structure of the deposited films, x-ray diffraction (XRD) was executed by a Bruker D8 Advance x-ray diffractometer with Cu $K\alpha$ ($\lambda \sim 1.5405$ Å) radiation. Furthermore, the element contents of the deposited films were analyzed by secondary ion mass spectrometry (SIMS, TOF-SIMS, IONTOF 5) and x-ray photoelectron spectroscopy (XPS) measurements (ESCALAB 250Xi, ThermoFisher Scientific). Moreover, ultraviolet visible (UV-vis) absorption spectrum was utilized to investigate the absorbance and calculate the optical bandgap of the Si-doped Ga_2O_3 films. Spectroscopic ellipsometry (SE) (SE-VE, Eoptics) was performed to estimate the thickness of the deposited films, and the ellipsometry measurement was performed with a wavelength ranging from 400 nm to 800 nm at an incidence angle of 65°. To further study the photoelectric behavior of the deposited films, an interdigital Ti/Au electrode was grown on the Si-doped Ga_2O_3 films through standard photolithography, magnetron sputtering deposition, and lift-off process successively. As shown in Fig. 4(a), the interdigital electrode was composed of 54 pairs of electrode fingers, and the length, width, and space gap of the electrode fingers were designed as 3300 μm, 10 μm, and 20 μm, respectively. The Ti/Au electrode was grown by magnetron sputtering and the thickness of Ti/Au was around 20 nm/70 nm. After the device was fabricated, Keithley 4200 semiconductor characterization system was employed to investigate the electric and photoelectric properties, while a UV lamp was placed over the device to provide 254 nm illumination.

3. Results and discussion

As shown in Fig. 1(a), Si-doped Ga_2O_3 films grown on (0001) Al_2O_3 substrates have a monoclinic β phase crystal structure as determined by XRD θ–2θ scan (JCPDS card No. 43-1012). In addition to the diffraction peak of the sapphire substrate, three main peaks located at around 18.90°, 38.32°, 59.0° are observed and can be assigned as ($\bar{2}$ 0 1), ($\bar{4}$ 0 2), ($\bar{6}$ 0 3) planes of β-Ga_2O_3.[40] Moreover, peaks with relatively low intensity are found at around 44.59° and 60.4°, which can be ascribed to the ($\bar{6}$ 0 1) and ($\bar{8}$ 0 1) planes of β-Ga_2O_3, indicating that the films grown by MOCVD under this deposition condition mainly are poly-crystalline with the doping of Si elements. Figure 1(b) displays the UV-vis absorbance of the Si-doped Ga_2O_3 films. From the profiles, it can be found that the sample shows a significant absorption edge at around 268 nm while exhibiting no obvious absorbance in UV-B, UV-A, and visible regions. Hence, $(\alpha h\nu)^2$ is plotted against the photon energy ($h\nu$) in the inset and the optical band gap is extracted to be 4.75 eV by fitting the linear region. The results imply that the doped Si element does not significantly change the absorption edge and the optical band gap of the Ga_2O_3 films. Moreover, XPS and SIMS measurements were utilized to further identify the chemical components of the films. Before analyzing the XPS results, the charge shift spectrum is calibrated through the core level energy of C 1s from the surface absorbate.

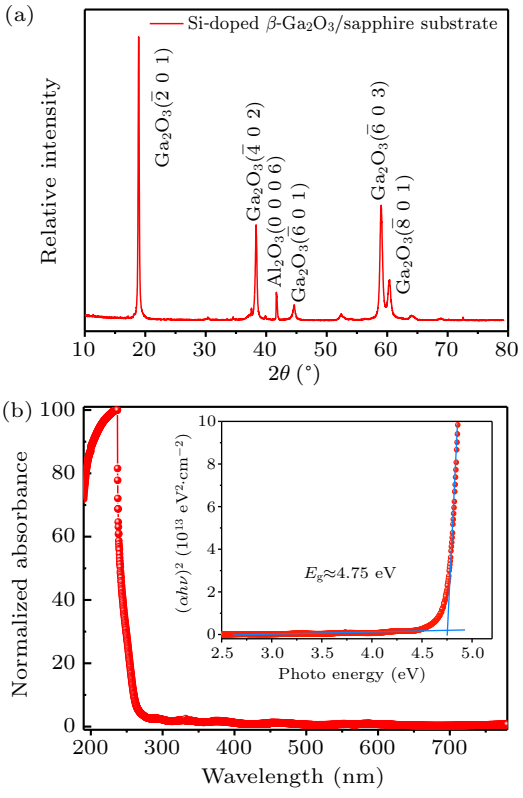


Fig. 1. (a) XRD scan and (b) UV-vis absorbance spectrum of the deposited Si-doped Ga_2O_3 films. The corresponding plot of $(\alpha h\nu)^2$ versus $h\nu$ for the sample is shown in the inset.

To find of the Si signal in XPS spectra, a fine scan was carried out in the range of 90–173 eV with a measuring step of 0.05 eV, and the results are displayed in Fig. 2(a). As shown in this figure, the black line-symbol plot represents the original measured data, while the red line and the green line represent the fitting curve and the background, respectively. From the fitting curve, it can be found that the XPS peaks at ∼ 105.7 eV and ∼ 109.3 eV could be divided into three components: Ga 3p 1/2 (109.2 eV), Ga 3p 3/2 (105.7 eV), and Si 2p (102.7 eV). The peak at around 161.1 eV is deduced to be Ga 3s (161 eV). In addition, a small peak at around 153.7 eV is derived from Si 2s (153.7 eV) from the XPS fitting results. Furthermore, compositions as a function of the film thickness are presented in the SIMS depth profile in Fig. 2(b), intensities of both Si and Ga ion counts remain almost constant, indicating that Si is actually uniformly distributed in the Si-doped Ga_2O_3 film. Combined with the XRD results, it can be concluded that the deposited films are mainly composed of Ga_2O_3 components and Si dopant instead of other element forms.

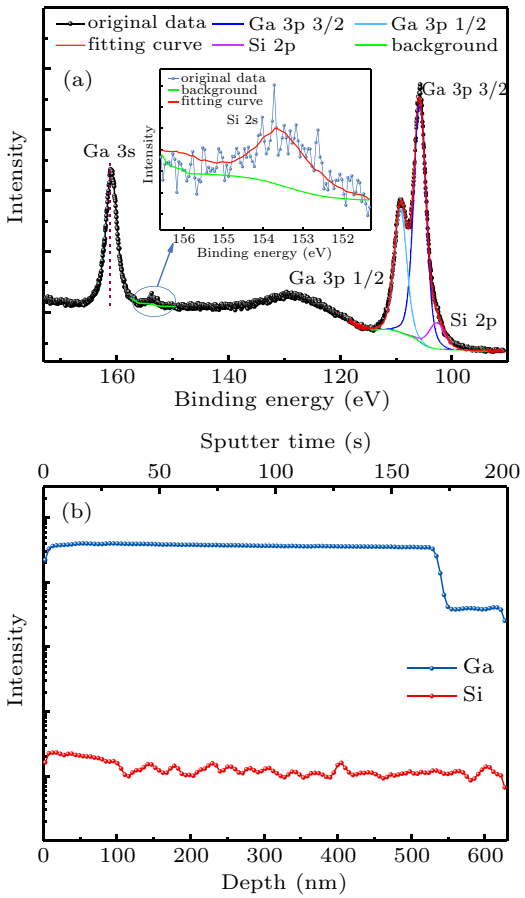


Fig. 2. (a) XPS spectra fine scan of the Si-doped Ga_2O_3 films ranging from 90 eV to 173 eV. (b) SIMS depth profiles of Si and Ga elements in the Si-doped Ga_2O_3 thin films.

Figure 3 presents the spectroscopic ellipsometry data for the grown films. In SE measurement, as the light reflects from the sample, its polarization changes, which can be described by an amplitude ratio (Ψ) and a phase difference (Δ). They are investigated by the equipment, and the film thickness and refractive index (n) could be deduced through a model fitting of the measured data.[41] As shown in Fig. 3(a), Ψ (red line) and Δ (blue line) are measured for a light wavelength ranging from 400 nm to 800 nm. Due to the excellent transparency of the Ga_2O_3 films in the measured wavelength range, Cauchy relation is used as the ellipsometric analysis model to simulate the SE results[42]

$$n(\lambda) = A + \frac{B}{\lambda^2} + \frac{C}{\lambda^4}, \tag{1}$$

where λ is the wavelength, and A, B, and C are the correlated coefficients. As seen in Fig. 3(a), a nonlinear curve simulation (black short dash curve) is performed perfectly when A, B, and C are equal to 1.916, 0.007, and 0.0005, respectively. Moreover, the variations of the refractive index (n) and extinction coefficient (k) with wavelength are obtained during the SE analysis. As shown in Fig. 3(b), the extinction coefficients of the Si-doped Ga_2O_3 films are set to zero and the refractive index n decreases slightly from 1.98 to 1.92, which are in agreement with the reported results.[41,43] With the SE measurement and analysis, the thickness of the deposited Si-doped Ga_2O_3 films is estimated to be 532.4 nm. The thickness of the films suggests that the device could efficiently absorb the illumination in the UVC range.[44]

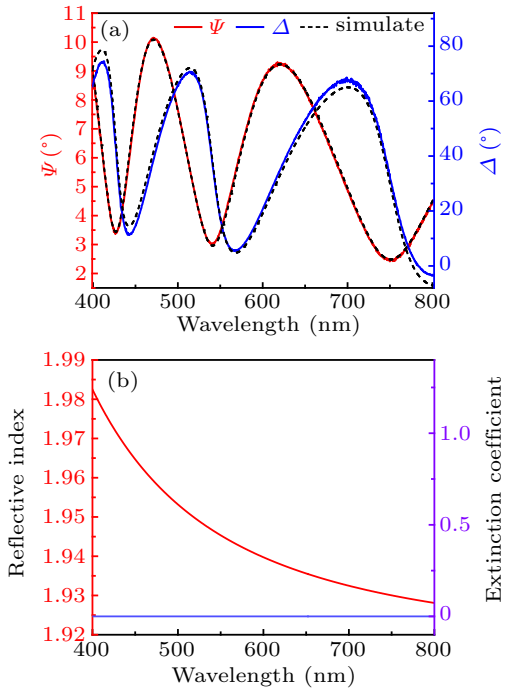


Fig. 3. (a) SE signals Ψ (red line) and Δ (blue line) for β-Ga_2O_3 films at an incidence angle of 65.48°. The black short dash curve represents the simulated data produced by Cauchy model. (b) Refractive index n and extinction coefficient k of the β-Ga_2O_3 thin films.

As for the photoelectric properties, the carrier transport behavior of the device is measured by 4200 sourcemeter instrument under various illumination environments, and the results are plotted in Fig. 4. Figure 4(b) displays the current–voltage correlations under dark, 365 nm, and 254 nm radia-

tion. It can be seen in the inset of Fig. 4(b) that the dark current (I_{dark}) of the device increases linearly with the voltage, suggesting good Ohmic contact between Ti/Au electrode and Si-doped Ga_2O_3 films. The resistivity of the device is calculated to be 0.55 MΩ, which is smaller than the majority of undoped Ga_2O_3 films (∼ TΩ). Hence it can be concluded that the dopant Si elements have efficiently enhanced the electric conductivity of the Ga_2O_3 films. Moreover, the device shows slight photo-response under 365 nm illumination with a photo-to-dark current ratio of ∼ 6. When the films are exposed under 254 nm radiation, the photo-current approaches 16 mA under 20 V bias, which is two orders of magnitude larger than that measured in dark. Figure 4(c) illustrates the detailed photo-electrical characteristics of the device under different illumination intensities. As the light intensity increases from 200 μW/cm^2 to 2000 μW/cm^2, the photo-current I_{photo} increases gradually from 11.2 mA to 21.7 mA at the bias of 20 V. In order to quantitatively gauge the optoelectrical properties of the photodetector, the responsivity of the device is calculated, and the results are drawn in Fig. 4(d). The responsivity, which is a basic parameter to evaluate how well the photo-generated electron–hole pairs are generated, can be figured out by the following equation:[15]

$$R = \frac{I_{photo} - I_{dark}}{PS}, \tag{2}$$

where P is the light intensity and S is the effective irradiated section of the device. According to the schematic diagram of the device, the effective area is calculated to be 3.57×10^{-2} cm^2. As seen in Fig. 4(d), when the device is exposed under 254 nm UV illumination with a light intensity of 200 μW/cm^2, the responsivity ranges from 5.6 A/W to 788.9 A/W with the increase of the voltage. As the responsivity results are compared under the same applied voltage, it is found that the responsivity declines slightly with the increase of the light intensity. This phenomenon could be ascribed to the larger phonon–electron scattering and higher electron–hole recombination possibility induced by the self-heating behavior at the higher light intensity and the larger concentration of non-equilibrium carriers.[20,45] From these phenomena, it can be concluded that the Si-doped Ga_2O_3 films exhibit excellent photo-response properties in the solar-blind region.

To assess the transient response time of the device, the time-dependent photo-response of the device is investigated with on/off switching of 254 nm light under various conditions, and the results are present in Fig. 5.

Figure 5(a) illustrates the current of the device under varied light intensities at the forward voltage of 1 V. When the 200 μW/cm^2 254 nm radiation is turned on, the current goes up instantaneously to 0.39 mA. After the light is turned off, the current descends immediately. With the increase of the 254 nm light intensity, the photo-current of the detector rises monotonically from 0.39 mA to 0.94 mA. Moreover, when the films are exposed to 254 nm illumination with the light intensity of 1000 μW/cm^2, the time-dependent photo-response diagram with various applied voltage is depicted in Fig. 5(b).

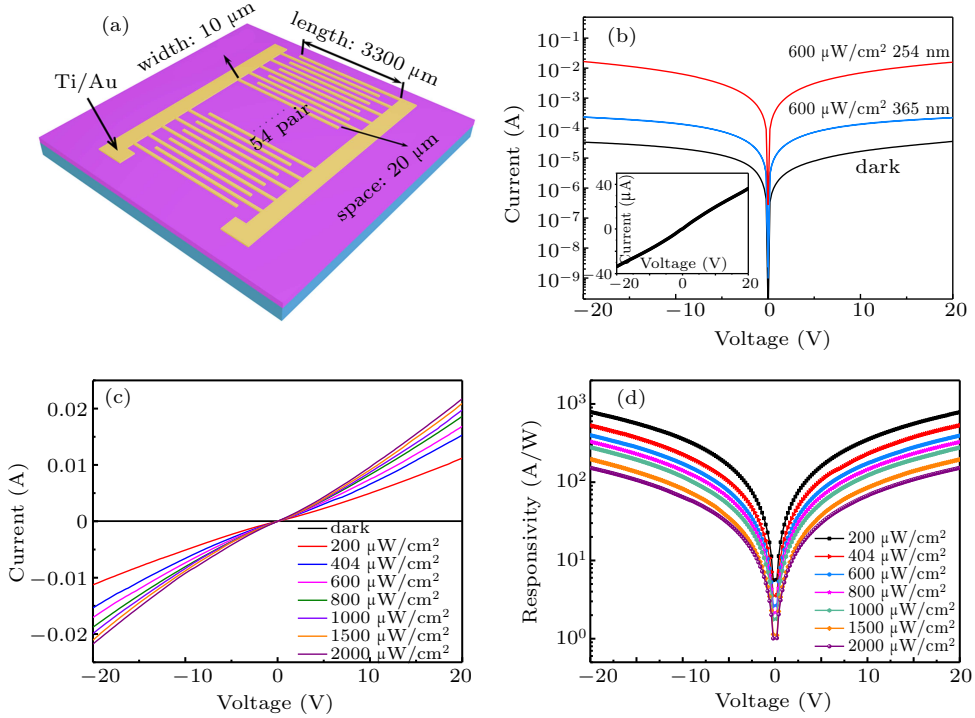


Fig. 4. (a) Schematic diagram of the MSM structured Si-doped Ga_2O_3 photodetectors. (b) Semi-logarithmic *I–V* characteristics of the device under dark, 365 nm, and 254 nm illumination, the inset shows the corresponding *I–V* curve under the dark condition in linear scale. (c) Linear scale *I–V* behaviors of the device under 254 nm illumination with the intensity increased from 200 μW/cm^2 to 2000 μW/cm^2. (d) Detailed responsivity of the photodetector to 254 nm radiation under various light intensities.

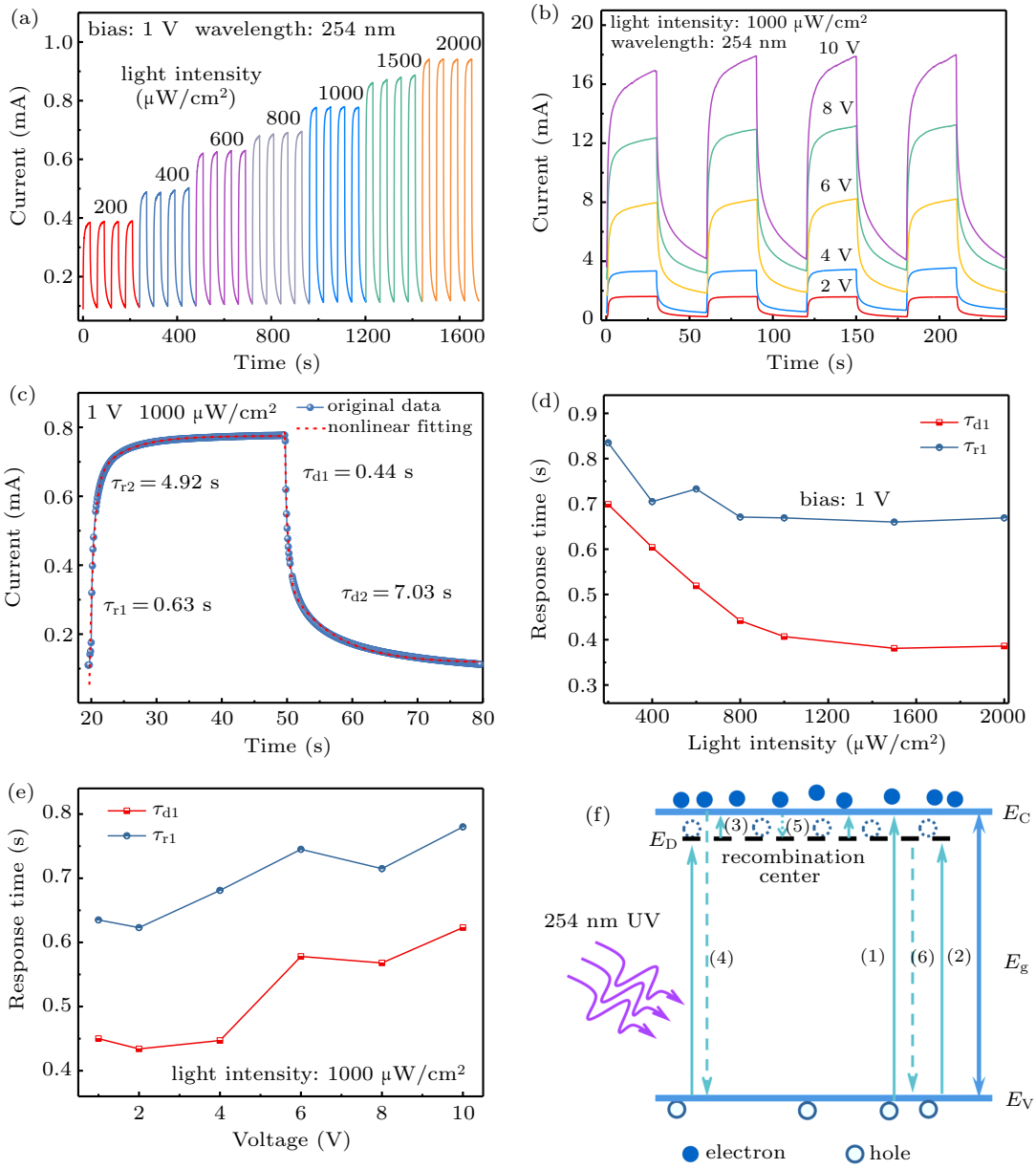


Fig. 5. The time-dependent photo-response of the detector (a) at 1 V bias under 254 nm illuminations with various light intensities, (b) under 1 mW/cm^2 254 nm UV light illumination at various biases. (c) The original transient response data and nonlinear fitting about the rise and decay time of the device. (d) Response time of the device under various light intensities at a bias of 1 V. (e) Response time of the device under various voltages under 1000 μW/cm^2 254 nm illumination. (f) Schematic diagram illustrating the photoelectric mechanism in Si-doped Ga_2O_3 films.

With the increase of the applied voltage, the photo-current of the Si-doped Ga_2O_3 films increases from 1.5 mA to 17.9 mA correspondingly. Stable photo-response characteristic in Figs. 5(a) and 5(b) shows that the device exposed under various light intensities can be switched between on and off states with good reproducibility. Furthermore, the response time could be deduced by the fitting rise and decay edges of the time-dependent photo-response curve with a biexponential relaxation equation[10]

$$I = I_0 + A\mathrm{e}^{-t/\tau_1} + B\mathrm{e}^{-t/\tau_2}, \tag{3}$$

where I represents the stable photo-current, A and B are constants, τ_1 and τ_2 are two relaxation time constants. The rise time and decay time of the photodetector are denoted by τ_r and τ_d, respectively. To quantitatively extrapolate the response time in rise edge and decay edge, one cycle of the time-dependent photo-response of the device at 1 V bias and 1000 μW/cm^2 circumstance is extracted, and the fitting results are shown in Fig. 5(c). It is clear that the rise time (τ_{r1}) and decay time (τ_{d1}) of the Si-doped Ga_2O_3 films are 0.63 s and 0.44 s, respectively, indicating the decent response speed in UV detection. In addition, the response time of the device under various voltage and light intensity is figured out, and the results are plotted in Figs. 5(d) and 5(e). It can be found that the response time (τ_{d1} and τ_{r1}) decreases slowly with the increase of the light intensity, which may be attributed to the large carrier transport velocity.[46] Furthermore, the response time (τ_{d1} and τ_{r1}) increases gradually with the increase

of the applied voltage, which could be ascribed to the persistent photoconductivity effect of the Si-doped Ga_2O_3 films under high voltage.[47] To further elucidate the excellent photoresponse performance of the device, a schematic diagram is illustrated in Fig. 5(f). As Si elements are doped to Ga_2O_3 films, Si prefers substituting to the tetrahedral coordination of the Ga1 site, leading to systematical increase of free electron density.[48] Moreover, Si dopants also behave as efficient shallow donor levels (less than 50 meV) in the energy band diagram. In Fig. 5(d), the upward solid arrows represent the generation of non-equilibrium carriers, while the downward dashed arrows denote the pathway for the carriers' recombination. As the 254 nm UV illuminate on the Si-doped Ga_2O_3 films, electron–hole pairs are generated and drifted to the electrode by the outside voltage. During this process, some photogenerated electrons jump from the valence band to the conduction band (process (1)), some electrons jump to the donor level (process (2)) and then transit to the conduction band (process (2)) because of the relatively low activation energy ($\leq$ 50 meV). Hence more electron–hole pairs could be more easily generated. Meanwhile, doping Si elements may effectively reduce the contact resistance, and more photo-generated carriers could be transferred to the outside electrode before recombination again. Thus, the device exhibits a larger photocurrent and responsivity. Ga_2O_3 film-based PDs are summarized in Table 1.[27,30,31,34,35,37,49] Compared with pure Ga_2O_3 and Ga_2O_3 doped with various impurities, Si-doped Ga_2O_3 films in this work give decent response time and large photocurrent (up to mA order of magnitude), leading to large responsivity (up to 788 A/W). It is noted that the performance of the Si-doped Ga_2O_3 based photodetector may also be enhanced by optimizing the fabrication parameters of the films or the structure of the photodetector.

Table 1. A brief summary of film-based Ga_2O_3 photodetectors.

Type	Grown method	Rise time (s)	Decay time (s)	Bias (V)	Responsivity (A/W)	Reference
β-Ga_2O_3/sapphire	MOCVD	0.48	0.18	1	26.1	[49]
α-Sn doped Ga_2O_3/sapphire	MBE	3.88	8.73	5	–	[27]
Si doped $(In_xGa_{1-x})_2O_3$/sapphire	PLD	–	–	–4	0.3	[30]
Mg doped Ga_2O_3/sapphire	RF-magnetron sputtering	0.33	0.02	1	0.024	[35]
Al doped Ga_2O_3/sapphire	MBE	1.26	1.99	1	1.4	[31]
Zn doped Ga_2O_3/sapphire	MOCVD	3.2	1.4	2	210	[34]
Si implanted Ga_2O_3/sapphire	MOCVD	0.58	1.2	5	1.45	[37]
Si doped Ga_2O_3/sapphire	MOCVD	0.78	0.62	1	350 (10 V) 788 (20 V)	this work

4. Conclusion

The Si-doped Ga_2O_3 films based MSM structured solar-blind photodetector is demonstrated. The refractive index of the grown films is extracted to be 1.98–1.92 by spectroscopic ellipsometry measurement. The device gives large photocurrent ranging from 11.2 mA to 21.7 mA at 20 V bias and high photo-responsivity of 788 $A{\cdot}W^{-1}$ under the illumination of 200 $\mu W{\cdot}cm^{-2}$ intensity. Moreover, the rise and decay relaxation times are found to be 0.63 s and 0.44 s, indicating a decent response to UV illumination. All these results suggest the promising future in solar-blind photodetectors.

References

[1] Chen H Y, Liu K W, Hu L F, Al-Ghamdi A A and Fang X S 2015 *Mater. Today* **18** 493
[2] Razeghi M and Rogalski A 1996 *J. Appl. Phys.* **79** 7433
[3] Xie C, Lu X T, Tong X W, Zhang Z X, Liang F X, Liang L, Luo L B and Wu Y C 2019 *Adv. Funct. Mater.* **29** 1806006
[4] Razeghi M 2002 *Proc. IEEE* **90** 1006
[5] Oshima T, Okuno T, Arai N, Suzuki N, Hino H and Fujita S 2009 *Jpn. J. Appl. Phys.* **48** 011605
[6] Chen X, Ren F, Gu S and Ye J 2019 *Photon. Res.* **7** 381
[7] Galazka Z 2018 *Semicond. Sci. Technol.* **33** 113001
[8] Chen Y C, Lu Y J, Liao M Y, Tian Y Z, Liu Q, Gao C J, Yang X and Shan C X 2019 *Adv. Funct. Mater.* **29** 1906040
[9] Xu J J, Zheng W and Huang F 2019 *J. Mater. Chem. C* **7** 8753
[10] Guo D Y, Wu Z P, Li P G, An Y H, Liu H, Guo X C, Yan H, Wang G F, Sun C L, Li L H and Tang W H 2014 *Opt. Mater. Express* **4** 1067
[11] Guo D Y, Zhao X L, Zhi Y S, Cui W, Huang Y Q, An Y H, Li P G, Wu Z P and Tang W H 2015 *Mater. Lett.* **164** 364
[12] Liu Z, Huang Y Q, Zhang C, Wang J, Li H R, Wu Z P, Li P G and Tang W H 2020 *J. Phys. D: Appl.Phys.* **53** 295109
[13] Cui S, Mei Z, Zhang Y, Liang H and Du X 2017 *Adv. Opt. Mater.* **5** 1700454
[14] Chen Y C, Lu Y J, Liu Q, Lin C N, Guo J, Zang J H, Tian Y Z and Shan C X 2019 *J. Mater. Chem. C* **7** 2557
[15] Liu Z, Zhi Y, Li S, Liu Y, Tang X, Yan Z, Li P, Li X, Guo D, Wu Z and Tang W 2019 *J. Phys. D: Appl. Phys.* **53** 085105
[16] Liu Z, Zhi Y, Zhang S, Li S, Yan Z, Gao A, Zhang S, Guo D, Wang J, Wu Z, Li P and Tang W 2020 *Science China-Technological Sciences* **64** 59
[17] Guo X C, Hao N H, Guo D Y, Wu Z P, An Y H, Chu X L, Li L H, Li P G, Lei M and Tang W H 2016 *J. Alloys Compd.* **660** 136
[18] Li S, Yan Z, Liu Z, Chen J, Zhi Y, Guo D, Li P, Wu Z and Tang W 2020 *J. Mater. Chem. C* **8** 1292
[19] Wang Y, Yang Z, Li H, Li S, Zhi Y, Yan Z, Huang X, Wei X, Tang W and Wu Z 2020 *ACS Appl. Mater. Interfaces* **12** 47714
[20] Kong W Y, Wu G A, Wang K Y, Zhang T F, Zou Y F, Wang D D and Luo L B 2016 *Adv. Mater.* **28** 10725
[21] Chen Y C, Lu Y J, Lin C N, Tian Y Z, Gao C J, Dong L and Shan C X 2018 *J. Mater. Chem. C* **6** 5727
[22] Qin Y, Dong H, Long S B, He Q M, Jian G Z, Zhang Y, Zhou X Z, Yu Y T, Hou X H, Tan P J, Zhang Z F, Liu Q, Lv H B and Liu M 2019 *IEEE Electron Device Lett.* **40** 742
[23] Qin Y, Long S B, He Q M, Dong H, Jian G Z, Zhang Y, Hou X H, Tan P J, Zhang Z F, Lu Y J, Shan C X, Wang J L, Hu W D, Lv H B, Liu Q and Liu M 2019 *Adv. Electron. Mater.* **5** 1900389

[24] Zhao X L, Cui W, Wu Z P, Guo D Y, Li P G, An Y H, Li L H and Tang W H 2017 *J Electron Mater* **46** 2366
[25] Zhao X, Wu Z, Guo D, Cui W, Li P, An Y, Li L and Tang W 2016 *Semicond. Sci. Technol.* **31** 065010
[26] Shu T K, Miao R X, Guo S D, Wang S Q, Zhao C H and Zhang X L 2020 *Chin. Phys. B* **29** 126301
[27] Zhao X L, Wu Z P, Cui W, Zhi Y S, Guo D Y, Li L H and Tang W H 2017 *ACS Appl. Mater. Interfaces* **9** 983
[28] Kokubun Y, Abe T and Nakagomi S 2010 *Phys. Status Solidi A* **207** 1741
[29] Tian W, Zhi C Y, Zhai T Y, Chen S M, Wang X, Liao M Y, Golberg D and Bando Y 2012 *J. Mater. Chem.* **22** 17984
[30] Zhang Z P, von Wenckstern H, Lenzner J, Lorenz M and Grundmann M 2016 *Appl. Phys. Lett.* **108** 123503
[31] Cui W, Guo D Y, Zhao X L, Wu Z P, Li P G, Li L H, Cui C and Tang W H 2016 *RSC Adv.* **6** 100683
[32] Wang C C, Yuan S H, Ou S L, Huang S Y, Lin K Y, Chen Y A, Hsiao P W and Wuu D S 2018 *J. Alloys Compd.* **765** 894
[33] Zhao X, Wu Z, Zhi Y, An Y, Cui W, Li L and Tang W 2017 *J. Phys. D: Appl.Phys.* **50** 085102
[34] Alema F, Hertog B, Ledyaev O, Volovik D, Thoma G, Miller R, Osinsky A, Mukhopadhyay P, Bakhshi S, Ali H and Schoenfeld W V 2017 *Phys. Status Solidi A* **214** 1600688
[35] Qian Y P, Guo D Y, Chu X L, Shi H Z, Zhu W K, Wang K, Huang X K, Wang H, Wang S L, Li P G, Zhang X H and Tang W H 2017 *Mater. Lett.* **209** 558
[36] Jiang Z X, Wu Z Y, Ma C C, Deng J N, Zhang H, Xu Y, Ye J D, Fang Z L, Zhang G Q, Kang J Y and Zhang T Y 2020 *Materials Today Physics* **14** 100226
[37] Oh S, Jung Y, Mastro M A, Hite J K, Eddy C R Jr and Kim J 2015 *Opt. Express* **23** 28300
[38] Ahn S, Ren F, Oh S, Jung Y, Kim J, Mastro M A, Hite J K, Eddy C R and Pearton S J 2016 *J. Vac. Sci. Technol. B* **34** 041207
[39] Alema F, Hertog B, Mukhopadhyay P, Zhang Y W, Mauze A, Osinsky A, Schoenfeld W V, Speck J S and Vogt T 2019 *APL Mater.* **7** 022527
[40] Xu C X, Liu H, Pan X H and Ye Z Z 2020 *Optical Materials* **108** 110145
[41] Zhao M L, Tong R J, Chen X H, Ma T C, Dai J, Lian J and Ye J D 2020 *Optical Materials* **102** 109807
[42] Ramachandran R K, Dendooven J, Botterman J, Sree S P, Poelman D, Martens J A, Poelman H and Detavernier C 2014 *Journal of Materials Chemistry A* **2** 19232
[43] O'Donoghue R, Rechmann J, Aghaee M, Rogalla D, Becker H W, Creatore M, Wieck A D and Devi A 2017 *Dalton Transactions* **46** 16551
[44] Wang X, Chen Z W, Guo D Y, Zhang X, Wu Z P, Li P G and Tang W H 2018 *Opt. Mater. Express* **8** 2918
[45] Li S, Guo D Y, Li P G, Wang X, Wang Y H, Yan Z Y, Liu Z, Zhi Y S, Huang Y Q, Wu Z P and Tang W H 2019 *ACS Appl. Mater. Interfaces* **11** 35105
[46] Liu Z, Li S, Yan Z Y, Liu Y Y, Zhi Y S, Wang X, Wu Z P, Li P G and Tang W H 2020 *J. Mater. Chem. C* **8** 5071
[47] Zhang Y F, Chen X H, Xu Y, Ren F F, Gu S L, Zhang R, Zheng Y D and Ye J D 2019 *Chin. Phys. B* **28** 028501
[48] Zhang J Y, Shi J L, Qi D C, Chen L and Zhang K H L 2020 *APL Mater.* **8** 020906
[49] Zhang D, Zheng W, Lin R C, Li T T, Zhang Z J and Huang F 2018 *J. Alloys Compd.* **735** 150